Rock Salt−Spinel Structural Transformation in Anodically Electrodeposited Mn−Co−O Nanocrystals

Weifeng Wei,* Weixing Chen, and Douglas G. Ivey

Department of Chemical and Materials Engineering, University of Alberta, Edmonton, Alberta, Canada T6G 2G6

Received December 5, 2007

Mn−Co−O nanocrystals, with a defective rock salt-type structure, were prepared by anodic electrodeposition. The structural and chemical stability of the as-deposited oxide nanocrystals were investigated using wavelength dispersive spectroscopy (WDS), X-ray photoelectron spectroscopy (XPS), and transmission electron microscopy (TEM). The rock salt−spinel structural transformation occurred in the oxide nanocrystals annealed at a temperature of 500 °C. A cubic $Fd\bar{3}m$ spinel-type structure was obtained in the Co-rich, Mn−Co−O oxide nanocrystals, while a distorted tetragonal-type spinel phase with a space group of $I4_1/amd$, induced by the Jahn–Teller effect, formed in their Mn-rich counterparts. It is noted that the structural transformation involves the migration of Mn/Co cations from the octahedral interstices to the tetrahedral interstices, which is accompanied by the reduction of Mn/Co cations and oxygen evolution. A novel mechanism for the structural transformation and reaction scheme is proposed in this work.

Introduction

Transition-metal oxide and spinel nanocrystals are of great interest, owing to their unique physicochemical properties and many potential technical applications, resulting from grain-size effects.[1–5] Because of their reduced size, these nanocrystals possess distinct morphologies, crystal structures, cation distributions, and oxidation states in comparison to the corresponding bulk materials, which may introduce novel and/or improved physicochemical properties. For instance, CoO typically forms as a stable rock salt cubic structure (space group of $Fm\bar{3}m$) with Co^{2+} in octahedral positions. However, CoO nanocrsytals, with a zinc blende structure, formed through the decomposition of Co acetate in a nitrogen atmosphere have been prepared.[6] Cobalt cations occupy half of the eight tetrahedral interstices in the zinc blende unit cell. Moreover, nanocrystalline CoO with a wurtzite ($P6_3mc$) hexagonal structure has also been prepared by decomposition of $Co(acetylacetonate)_2$ in refluxing benzyl ether or decomposition of $Co(acetylacetonate)_3$ in oleylamine.[7,8] These new CoO nanocrystals, particularly the wurtzite structure, are expected to have anomalous magnetic properties.[9,10] The metastable wurtzite structure transforms into the stable rock salt structure, in nanocrystalline CoO, by a nucleation and growth mechanism at a temperature of 200 °C.[11]

Grain-size effects on structural and chemical stability were also noted in Mn−Co oxides, $Mn_xCo_{3-x}O_4$ ($0 < x < 3$). For high-temperature ceramic processes (1000 °C) and moderate temperature thermal decomposition (400 °C) procedures,[12–15] a cubic $Fd\bar{3}m$ spinel-type solid solution is formed in the compositional range of $0 < x < 1.3$ and a tetragonal $I4_1/amd$ single phase is formed in the interval $1.9 < x < 3.0$. $Mn_xCo_{3-x}O_4$ phases are mixtures of cubic and tetragonal spinel-type structures for intermediate compositions ($1.3 < x < 1.9$). Low-temperature procedures (80–200 °C), e.g., spinel-type cobalt manganese oxides by coprecipitation with butylamine of mixed Co^{II}/Mn^{II} chloride solutions, have been reported to increase the upper limit for the cubic $Fd\bar{3}m$ spinel-like phase to $x = 1.4$ and the lower limit for the tetragonal $I4_1/amd$ spinel-type phase to $x = 2.0$, respectively.[16–19] Recently, amorphous and hydrated Mn−Co binary oxide coatings have been synthesized using electrodeposition based on aqueous solutions at room temperature.[20] The high

* To whom correspondence should be addressed. E-mail: weifeng@ualberta.ca.

(1) Tarascon, J. M.; Armand, M. *Nature* **2001**, *414*, 359–367.
(2) Ross, C. *Annu. Rev. Mater. Res.* **2001**, *31*, 203–235.
(3) Zeng, H.; Li, J.; Liu, J. P.; Wang, Z. L.; Sun, S. *Nature* **2002**, *420*, 395–398.
(4) Kittilstved, K. R.; Liu, W. K.; Gamelin, D. R. *Nat. Mater.* **2006**, *5*, 291–297.
(5) Patolsky, F.; Weizmann, Y.; Katz, E.; Willner, I. *Angew. Chem., Int. Ed.* **2003**, *42*, 2372–2376.
(6) Redman, M. J.; Steward, E. G. *Nature* **1962**, *193*, 867.
(7) Risbud, A. S.; Snedeker, L. P.; Elcombe, M. M.; Cheetham, A. K.; Seshadri, R. *Chem. Mater.* **2005**, *17*, 834–838.
(8) Seo, W. S.; Shim, J. H.; Oh, S. J.; Lee, E. K.; Hur, N. H.; Park, J. T. *J. Am. Chem. Soc.* **2005**, *127*, 6188–6189.
(9) Dietl, T.; Ohno, H.; Matsukara, F.; Cibe'rt, J.; Ferrand, D. *Science* **2000**, *287*, 1019–1022.
(10) Ohno, H. *Science* **1998**, *281*, 951–956.
(11) Liu, J. F.; Yin, S.; Wu, H. P.; Zeng, Y. W.; Hu, X. R.; Wang, Y. W.; Lv, G. L.; Jiang, J. Z. *J. Phys. Chem. B* **2006**, *110*, 21588–21592.
(12) Buhl, R. *J. Phys. Chem. Solids* **1969**, *30*, 805–812.
(13) Boucher, B.; Buhl, R.; di Bella, R.; Perrin, M. *J. Phys.* **1970**, *31*, 113.
(14) Naka, S.; Inagaki, M.; Tanaka, T. *J. Mater. Sci.* **1972**, *7*, 441–444.
(15) Jimenez-Mateo, J. M.; Morales, J.; Tirado, J. L. *J. Solid State Chem.* **1989**, *82*, 87–94.
(16) Martin de Vidales, J. L.; Garcia-Martinez, O.; Vila, E.; Rojas, R. M.; Torralvo, M. J. *MRS Bull.* **1993**, *28*, 1135–1143.
(17) Rojas, R. M.; Vila, E.; Garcia-Martinez, O.; Martin de Vidales, J. L. *J. Mater. Chem.* **1994**, *4*, 1635–1639.
(18) Martin de Vidales, J. L.; Vila, E.; Rojas, R. M.; Garcia-Martinez, O. *Chem. Mater.* **1995**, *7*, 1716–1721.
(19) Vila, E.; Rojas, R. M.; Martin de Vidales, J. L.; Garcia-Martinez, O. *Chem. Mater.* **1996**, *8*, 1078–1083.

10.1021/cm703464p CCC: $40.75
Published on Web 01/19/2008

specific capacitance obtained in these oxide coatings was attributed to their amorphous and hydrous natures.

In previous papers, we have reported on Mn−Co−O nanocrystals with a defective rock salt structure prepared by anodic electrodeposition.[21,22] In this metastable rock salt structure, in addition to the metal cations (Co and Mn), a significant number of vacancies reside in the octahedral interstices of the face-centered cubic arrays of oxygen anions. To explore their properties and any potential applications, a clear understanding of the structural and chemical stability of these new Mn−Co−O nanocrystals is essential. The aim of this work is to study the structural and chemical evolution of the metastable Mn−Co−O phase after annealing in air. The purpose of this work is not only to obtain structural and chemical stability information for the novel structure Mn−Co−O nanocrystals but also to enhance the knowledge base for phase transitions in nanocrystalline oxides.

Experimental Procedure

The Mn−Co−O nanocrystals were deposited on ferritic stainless-steel substrates as described previously using anodic electrodeposition.[21,22] The solutions consisted of 0.2 M ethylenediaminetetraacetic acid (EDTA) disodium and various concentrations of $CoSO_4 \cdot 7H_2O$ and $MnSO_4 \cdot H_2O$. Several different Co^{II}/Mn^{II} mole ratios (pure Co^{II}, 29:1, 9:1, and pure Mn^{II}) were used, and the total metal ion concentration was set to 0.3 M. The deposition current density, pH value, and temperature of the solutions were adjusted to be 5 mA/cm^2, 6.0, and 70 °C, respectively. The oxide layers were grown to a thickness of 3–4 μm over a period of 80–90 min. After electrodeposition, the working electrodes were rinsed with deionized water, dried at 70 °C for 5 h in air, and then stored in a vacuum desiccator before further annealing and analysis. Heat treatment of the deposited Mn−Co−O nanocrystals was conducted in air at various temperatures ranging from 200 to 600 °C for 5 h.

Quantitative chemical analysis of the Mn−Co−O nanocrystals was conducted using a JEOL 8900 microprobe, equipped with five wavelength-dispersive spectrometers (WDSs). The microprobe was operated at an energy of 15 kV, with a beam current of 15 nA. The quantitative information for each sample was obtained by averaging 10 independent measurements. Chemical-state analysis was carried out by X-ray photoelectron spectroscopy (XPS) using a Kratos AXIS Ultra X-ray photoelectron spectrometer. A monochromatic Al source, operating at 210 W with a pass energy of 20 eV and a step of 0.1 eV, was used. All XPS spectra were corrected using the C 1s line at 284.6 eV. Curve fitting and background subtraction were accomplished using Casa XPS version 2.3.13 software.

The crystal structure and morphology of the as-deposited and annealed Mn−Co−O nanocrystals were investigated using transmission electron microscopy (TEM). Crystal structure analysis was performed using selected area diffraction (SAD) patterns obtained from the thinnest regions. Electron transparent samples were produced by scraping off the deposits and ultrasonically dispersing in methanol. One or two drops of the suspension were then deposited on C-coated Cu grids. After evaporation of the methanol, samples were ready for analysis.

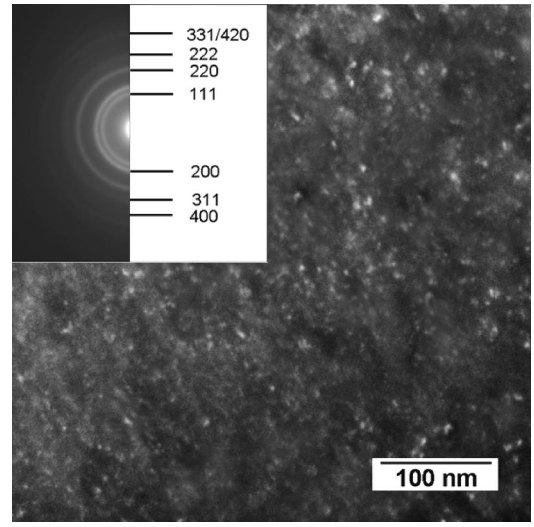

Figure 1. TEM DF micrograph of an as-deposited oxide prepared from a solution with a Co^{II}/Mn^{II} ratio of 29:1 (Co-rich). The inset is the SAD pattern from the region shown.

Electron diffraction and imaging were performed in a JEOL 2010 transmission electron microscope equipped with a Noran ultrathin window (UTW) X-ray detector.

Results and Discussion

A typical TEM dark field (DF) micrograph and a corresponding SAD pattern of an as-deposited Mn−Co−O nanocrystal sample, prepared from a solution with a Co^{II}/Mn^{II} ratio of 29:1, are shown in Figure 1. The DF micrograph reveals that the oxide is composed of nanocrystalline particles with diameters less than 10 nm. The corresponding electron diffraction pattern confirms the nanocrystalline nature and a face-centered cubic (FCC) symmetry. To determine the crystal structure of the as-deposited Mn−Co−O nanocystals, simulated electron diffraction patterns based on several possible FCC-type model structures were calculated in a previous study.[22] The intensity profiles of the experimental SAD ring patterns were observed to be consistent with that of simulated SAD ring pattern calculated from a defective rock salt-type structure.[22] This type of metastable structure can be described as an FCC array of oxygen anions, with Mn and Co cations randomly occupying the octahedral interstices. A significant number of cation vacancies also reside on the octahedral interstices in the FCC unit cell.[22] In these defective rock salt-type Mn−Co−O nanocrystals, ranging from pure $Co_{1-x}O$ to pure $Mn_{1-x}O$, the oxygen anion/metal cation ratios were calculated to be in the 1.47 to 1.79 range, [22] which is well in excess of the ratio for stable rock salt-type oxides (anion/cation ratio = 1) and spinel oxides (anion/cation ratio = 4:3). The formation of this type of defective rock salt-type structure is probably a consequence of the low-temperature process for electrodepositing the oxides.[22]

The structural stability of as-deposited oxide nanocrystals was mainly determined using TEM. Figure 2 shows TEM micrographs and SAD patterns of the oxide nanocrystals annealed at various temperatures in air. Table 1 summarizes their electron diffraction information. After 5 h at 200 and

(20) Chuang, P. Y.; Hu, C. C. *Mater. Chem. Phys.* **2005**, *92*, 138–145.
(21) Wei, W. F.; Chen, W.; Ivey, D. G. *Chem. Mater.* **2007**, *19*, 2816–2822.
(22) Wei, W. F.; Chen, W.; Ivey, D. G. *J. Phys. Chem. C* **2007**, *111*, 10398–10403.

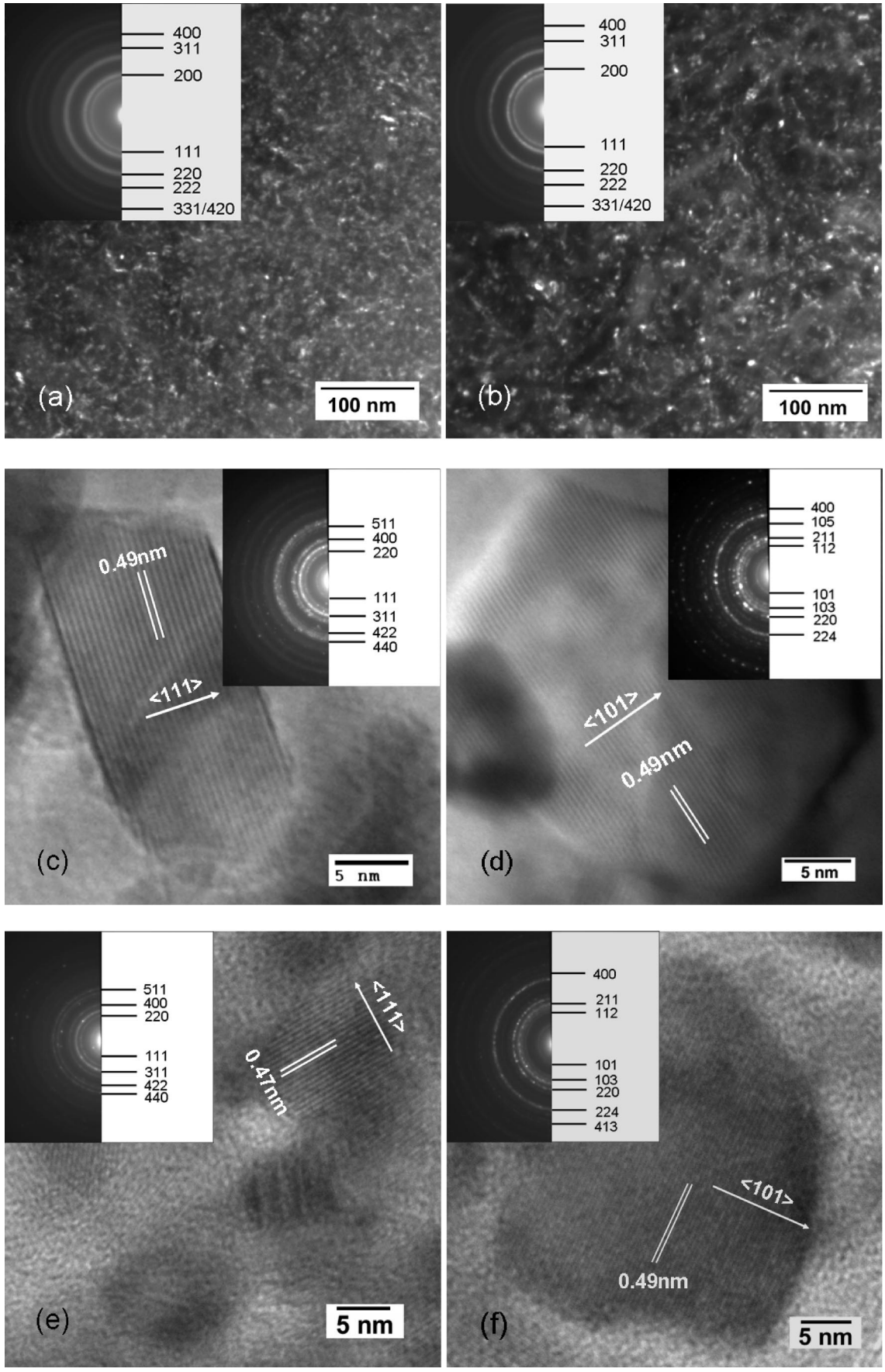

Figure 2. TEM micrographs for the oxide nanocrystals treated at various temperatures in air. (a) 29:1 Co/Mn, 200 °C; (b) 29:1 Co/Mn, 400 °C; (c) 29:1 Co/Mn, 500 °C; (d) 9:1 Co/Mn, 500 °C; (e) pure Co oxides, 500 °C; and (f) pure Mn oxides, 500 °C. Note that a and b are DF images.

400 °C (parts a and b and insets of Figure 2), the crystal structure remains the same as that for the as-deposited oxide (Figure 1). As the annealing temperature increases, there is an apparent decrease in the *d* spacings for the diffracted rings

Table 1. Electron Diffraction Information for the Oxide Nanocrystals Annealed at Various Temperatures

d spacing (nm)/Miller indices (*hkl*)						
	29:1 Co/Mn			9:1 Co/Mn	$Co_{1-x}O$	$Mn_{1-x}O$
as deposited	200 °C	400 °C	500 °C	500 °C	500 °C	500 °C
0.250/(111)	0.249/(111)	0.242/(111)	0.483/(111)	0.491/(101)	0.470/(111)	0.492/(101)
0.213/(200)	0.213/(200)	0.209/(200)	0.295/(220)	0.307/(112)	0.289/(220)	0.308/(112)
0.151/(220)	0.150/(220)	0.146/(220)	0.251/(311)	0.275/(103)	0.245/(311)	0.277/(103)
0.128/(311)	0.128/(311)	0.125/(311)	0.209/(400)	0.249/(211)	0.203/(400)	0.251/(211)
0.122/(222)	0.121/(222)	0.119/(222)	0.170/(422)	0.205/(220)	0.166/(422)	0.204/(220)
0.106/(400)	0.106/(400)	0.104/(400)	0.160/(511)	0.179/(105)	0.155/(511)	0.154/(224)
0.096/(331)/(420)	0.095/(331)/(420)	0.092/(331)/(420)	0.148/(440)	0.153/(224)	0.130/(440)	0.144/(400)
				0.143/(400)		0.127/(413)
SG[a] = $Fm\bar{3}m$	SG = $Fm\bar{3}m$	SG = $Fm\bar{3}m$	SG = $Fd\bar{3}m$	SG = $I4_1/amd$	SG = $Fd\bar{3}m$	SG = $I4_1/amd$
a = 0.428 nm	a = 0.427 nm	a = 0.416 nm	a = 0.831 nm	a = 0.576 nm	a = 0.811 nm	a = 0.576 nm
				c = 0.946 nm		c = 0.947 nm

[a] SG = space group.

(Table 1). Moreover, the crystallization degree and grain size also increase with increasing annealing temperature, which is clear because distinct spots are distinguishable in the high-temperature diffraction patterns (inset in Figure 2b). Further increasing the temperature to 500 °C leads to a phase transformation. The SAD pattern for the sample annealed at this temperature is different from those at lower annealing temperatures and can be indexed to the cubic spinel structure, with a space group of $Fd\bar{3}m$ (inset of Figure 2c). A high-resolution TEM (HRTEM) image of an isolated spinel Mn−Co−O nanocrystal is shown in Figure 2c, where the *d* spacing of 0.490 nm corresponds to the (111) plane for the cubic spinel phase (Table 1). The grain size has also increased from several nanometers for the as-deposited oxide nanocrystals to several tens of nanometers for the oxide nanocrystals annealed at 500 °C.

For Mn-rich, Mn−Co−O nanocrystals prepared from a solution with a Co^{II}/Mn^{II} ratio of 9:1, the rock salt−spinel structural transformation also occurred. However, careful examination of the SAD pattern indicates that the crystal structure is not cubic but a distorted spinel phase, i.e., a tetragonal-type spinel with a space group of $I4_1/amd$ (inset of Figure 2d and Table 1). This means that the increase in the Mn content in the oxide nanocrystals induces the distorted spinel phase, likely through the Jahn–Teller effect.[23] This is further confirmed by the rock salt−tetragonal spinel transformation, which occurs for pure Mn oxide nanocrystals treated at 500 °C (Figure 2f and inset). Figure 2e illustrates the rock salt−cubic spinel transformation for pure Co oxide nanocrystals treated at 500 °C. A cubic $Fd\bar{3}m$ spinel phase could be formed, as shown in the inset of Figure 2e. Therefore, the rock salt−spinel phase transition occurred for all Mn−Co−O nanocrystals treated at 500 °C for 5 h. The crystal structure for annealed Mn−Co−O nanocrystals is sensitive to their chemistry, specifically the Mn content, which is consistent with previous research.[18,19] Moreover, it is apparent that grain growth in spinel phases is also dependent upon the oxide chemistry; i.e., growth increases with increasing Mn content. This tendency is most likely related to the faster diffusion rate of Mn cations in the oxygen anion arrays when compared to that of Co cations.[24]

(23) Goodenough, J. B. *Annu. Rev. Mater. Sci.* **1998**, *28*, 1–27.
(24) Reed, J.; Ceder, G. *Chem. Rev.* **2004**, *104*, 4513–4534.

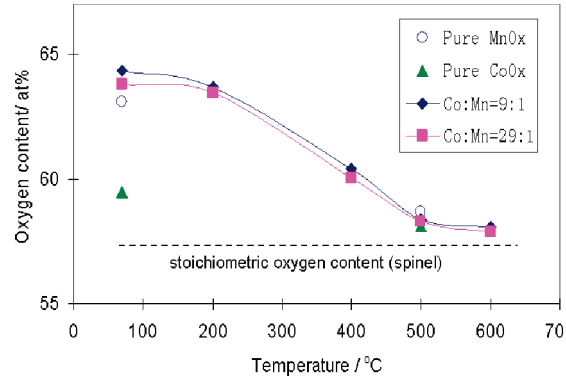

Figure 3. Quantitative WDS analysis of oxygen content in the oxide nanocrystals annealed at various temperatures.

The transformation of rock salt-type Mn−Co−O into spinel-type Mn−Co−O involves a rearrangement of cations (Mn or Co) from the octahedral interstices, characteristic of the rock salt-type structure, to the tetrahedral interstices, characteristic of the spinel-type structure. Considering that the oxygen anion/metal cation ratios of as-deposited Mn−Co−O nanocrystals are much higher than those of stable spinel Mn−Co−O phases (anion/cation ratio = 4:3),[22] rearrangement within the closed-packed oxygen anion lattices may also occur. To clarify the chemical evolution during the rock salt−spinel transformation, WDS and XPS were applied to determine the oxygen content change and the oxidation state evolution of cations in the Mn−Co−O nanocrystals during the structural transformation. Figure 3 depicts the oxygen content change for the oxide nanocrystals treated at various temperatures. For these oxide nanocrystals, regardless of chemistry, the oxygen content decreases continuously with increasing temperature and approaches the stoichiometric oxygen content for stable spinel phases. This implies that oxygen loss is induced by annealing the oxide nanocrystals in air. To further confirm this unusual reduction process occurred in air, a detailed chemical-state analysis for Mn and Co cations in the as-deposited and annealed oxide nanocrystals was conducted, shown as the XPS spectra in Figure 4.

The possible variations in oxidation states for Co can be determined from the Co 2p peaks in the XPS spectra. In parts a, c, and e of Figure 4, the Co 2p spectra consist of two main spin–orbital lines, i.e., $2p_{3/2}$ and $2p_{1/2}$, at ~780.3 and ~795.3 eV, separated by about 15.0 eV, as reported in

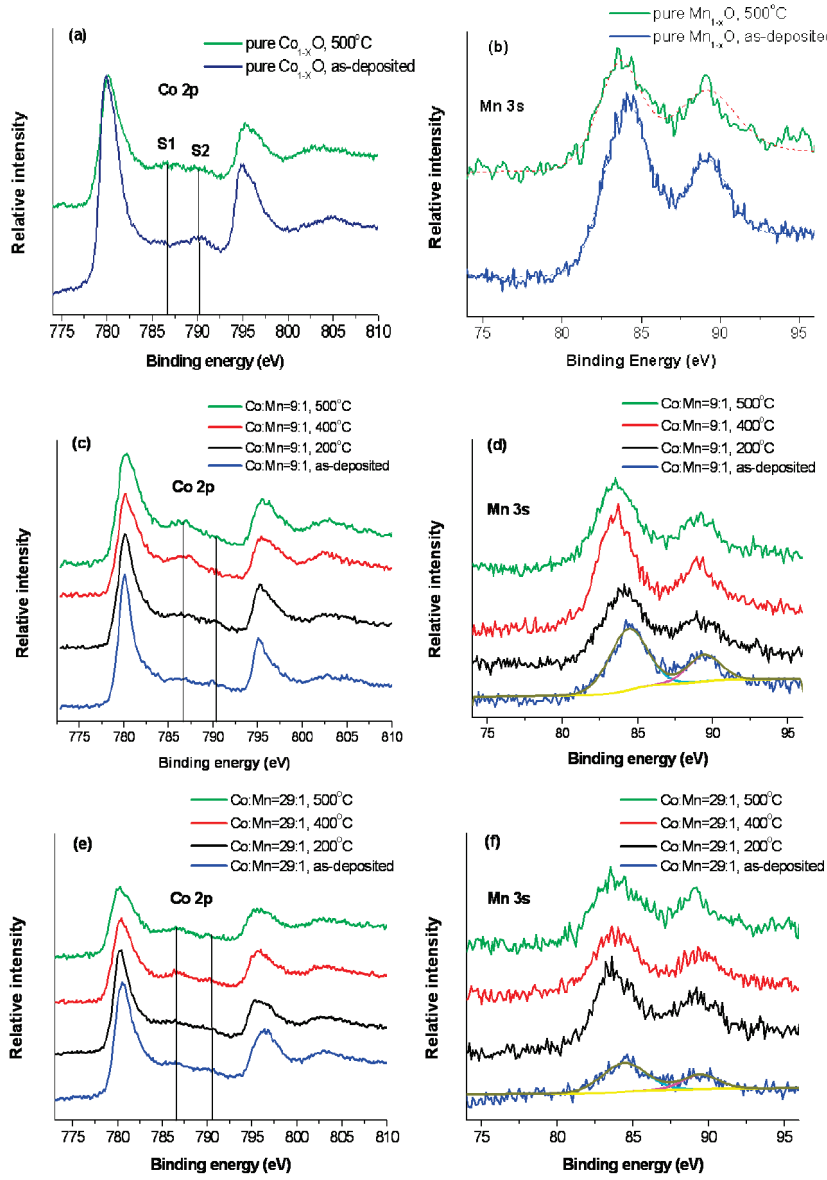

Figure 4. XPS spectra for Mn−Co−O oxides annealed at various temperatures.

the literature.[25–27] However, the determination of the oxidation states of Co cations is rather difficult, merely on the basis of the binding energy of Co 2p main peaks, because similar spectra can be obtained for CoO, Co_3O_4, and Co_2O_3 oxides. Therefore, information from the satellite peaks needs to be considered. It is generally accepted that the energy gap between the Co 2p main peak and the satellite peaks is highly related to the oxidation states. When the energy gap is ~6.0 eV, the Co cation valence is assigned a value of 2+. If the energy gap is 9−10 eV, the spectrum is associated with Co cations having a valence of 3+.[25–37] For the pure $Co_{1-x}O$ nanocrystals (Figure 4a), two distinguishable satellite peaks were detected at about 6 eV (S1) and 10 eV (S2) above the Co $2p_{3/2}$ main peak. The intensity of S1 is much weaker than that of S2, which means that Co^{3+} cations are the predominant species in the as-deposited $Co_{1-x}O$. However, the intensity of S1 is higher than that of S2 in the annealed $Co_{1-x}O$ nanocrystals. About half of the Co^{3+} cations have

(25) Kim, K. S. *Phys. Rev. B: Condens. Matter Mater. Phys.* **1975**, *11*, 2177–2185.
(26) Barreca, D.; Massignan, C.; Daolio, S.; Fabrizio, M.; Piccirillo, C.; Armealo, L.; Tondello, E. *Chem. Mater.* **2001**, *13*, 588–593.
(27) Gulino, A.; Fiorito, G.; Fragala, I. *J. Mater. Chem.* **2003**, *13*, 861–865.
(28) Gulino, A.; Dapporto, P.; Rossi, P.; Fragala, I. *Chem. Mater.* **2003**, *15*, 3748–3752.
(29) Pasko, S.; Abrutis, A.; Hubert-Pfalzgraf, L. G.; Kubilius, V. *J. Cryst. Growth* **2004**, *262*, 653–657.
(30) Pasko, S.; Hubert-Pfalzgraf, L. G.; Abrutis, A.; Vaissermann, J. *Polyhedron* **2004**, *23*, 735–741.
(31) Cataldi, T. R. I.; Gasella, I. G.; Desimoni, E.; Rotunno, T. *Anal. Chim. Acta* **1992**, *270*, 161–171.
(32) Valeri, S.; Borghi, A.; Gazzadi, G. C.; di Bona, A. *Surf. Sci.* **1999**, *423*, 346–356.
(33) Shen, Z. X.; Allen, J. W.; Lindberg, P. A. P.; Dessau, D. S.; Wells, B. O.; Borg, A.; Ellis, W.; Kang, J. S.; Oh, S. J. *Phys. Rev. B: Condens. Matter Mater. Phys.* **1990**, *42*, 1817–1828.
(34) Jimenez, V. M.; Fernendz, A.; Espinos, J. P.; Gonzalez-Elipe, A. R. *J. Electron Spectrosc. Relat. Phenom.* **1995**, *71*, 61–71.
(35) Ernst, B.; Libs, S.; Chaumette, P.; Kiennemann, A. *Appl. Catal., A* **1999**, *186*, 145–168.
(36) Gastner, D. G.; Watson, P. R.; Chan, I. Y. *J. Phys. Chem.* **1989**, *93*, 3188–3194.
(37) Burriel, M.; Garcia, G.; Santiso, J.; Abrutis, A.; Saltyte, Z.; Figueras, A. *Chem. Vap. Deposition* **2005**, *11*, 106–111.

Table 2. XPS Results from the Mn 3s Peak Showing Approximate Valence of the Oxide Nanocrystals Annealed at Various Temperatures

	pure $Mn_{1-x}O$		9:1 Co/Mn		29:1 Co/Mn	
	ΔE (eV)	valence of Mn	ΔE (eV)	valence of Mn	ΔE (eV)	valence of Mn
as deposited	5.02	3.54	5.01	3.48	5.05	3.48
200 °C			5.12	3.34	5.26	3.06
400 °C			5.36	2.86	5.49	2.60
500 °C	5.45	2.68	5.46	2.66	5.50	2.58

been reduced into Co^{2+} cations after annealing in air. For the as-deposited mixed Mn−Co oxides (9:1 and 29:1 Co/Mn), as shown in parts c and e of Figure 4, the intensity of S1 is slightly higher than that of S2; i.e., the number of Co^{2+} and Co^{3+} cations is comparable in the mixed Mn−Co oxides. With increasing annealing temperatures, the S1 satellite peaks (Co^{2+} cation content) became more distinct, whereas the S2 peaks were slightly suppressed. Deconvolution of the satellite peaks to obtain quantitative information for the Co^{3+} to Co^{2+} transition was not successful; however, it is reasonable to conclude that the reduction reaction for Co^{3+} to Co^{2+} cations occurred in these oxide nanocrystals.

The oxidation states for Mn in the oxide nanocrystals were determined by analyzing the Mn 3s XPS spectra. The doublet Mn 3s peaks are the result of parallel spin coupling between electrons in the 3s and 3d orbitals. The oxidation states for Mn are closely related to the 3s peak-splitting widths. When the valence of the Mn cations increases, i.e., less electrons exist in the 3d orbitals, the splitting width decreases.[38,39] Mn 3s spectra for pure Mn oxides and mixed Mn−Co oxides (9:1 and 29:1 Co/Mn) are shown in parts b, d, and f of Figure 4. On the basis of an approximately linear relationship between the splitting width (ΔE) and the Mn oxidation state,[38–41] the experimental splitting widths (ΔE) in the Mn 3s spectra were converted into average oxidation valences and tabulated in Table 2. XPS studies show that the oxidation state for Mn is a roughly even mixture of +3 and +4 valences in the as-deposited oxide nanocrystals. The Mn^{3+} and Mn^{4+} cations were gradually reduced to Mn^{2+} and Mn^{3+} as the oxide nanocrystals were annealed at temperatures up to 500 °C. Consistent results were obtained for independent samples with different chemical information. The reduction process for Co and Mn cations during annealing in air is due to the loss of oxygen anions from the oxide nanocrystals. This is consistent with the lower oxygen content in the annealed oxide nanocrystals determined from WDS results.

When the structural and chemical information are taken into account, it is noted that the rock salt−spinel structural transformation involves the migration of Mn/Co cations from the octahedral interstices to the tetrahedral interstices, which is accompanied by the reduction reactions for Mn and Co cations and the oxygen evolution reaction. Figure 5 illustrates the possible structural evolution and reaction scheme during the transformation from the defective rock salt structure to stable spinel structures. Here, it is assumed that the reduction reactions only occur for the migrating Mn/Co cations. The possible transformation processes could be depicted as follows: As the annealing temperature increases, some of the cations in the octahedral interstices have sufficient energy to overcome the energy barrier to migrate to the nearest neighbor tetrahedral vacancies, shown by the arrow in Figure 5. This kind of migration will generate vacancies in their previous octahedral positions. With an increase in cation vacancies, it is expected that the vacant octahedral sites will become more and more unfavorable energetically. Once the number of the vacant octahedral sites exceeds a certain threshold, some of them will collapse. This is verified by the decrease in *d* spacings for the diffraction patterns taken from samples annealed at higher temperatures (Table 1). The extra oxygen anions will form paired bonds to generate oxygen gas. Meanwhile, the migrating Mn/Co cations will capture the electrons released from the oxygen evolution reaction to maintain the charge balance in the oxides (Figure 5). Once one-eighth of the tetrahedral interstices in the FCC oxygen anion arrays are occupied by Mn/Co cations, the spinel-type structure will form. The polyhedra shown in Figure 5 are undistorted, which is not generally suitable to describe the rock salt−spinel transformation in the Mn-rich oxide nanocrystals. In this case, the octahedra are distorted by both the Mn cation ordering, which alters the cubic symmetry of the oxygen sublattice,[22] and the Jahn–Teller effect,[23] which induces the tetragonal spinel structure.

Given that the cation deficiency (percentage of vacancies) in the octahedral interstices in the as-deposited oxide nanocrystals is in the 30−45% range, the dangling bond density and the surface energy in the as-deposited oxide nanocrystals (less than 10 nm in diameter) would be extremely high, which may accelerate cation migration. Consistent data were obtained from the WDS and XPS results (Figure 3, Figure 4, and Table 2). Oxygen evolution and reduction of Co/Mn cations occurred even at temperatures as low as 200 °C. However, the same crystal structure was identified from the SAD patterns for the oxide nanocrystals annealed at 200 and 400 °C (parts a and b of Figure 2). Therefore, the rock salt−spinel structural transformation is a gradual process. The migration of Co/Mn cations, oxygen evolution and the reduction of cations are the necessary processes for spinel phase nucleation (Figure 5). In the metastable rock salt-type nanocrystals, the migration of Mn/Co cations will occur preferentially at the surface. Because a spinel unit cell is composed of eight rock salt-type subcells, a stable nucleus of the spinel phase can form on the oxide particle surface only when one-eighth of the tetrahedral interstices in these eight subcells is occupied by migrating cations. The spinel nuclei will grow and spread from the surface to the center of the rock salt-type nanocrystals over

(38) Carver, J. C.; Schweitzer, G. K.; Carlson, T. A. *J. Chem. Phys.* **1972**, *57*, 973–982.
(39) Chigane, M.; Ishikawa, M. *J. Electrochem. Soc.* **2000**, *147*, 2246–2251.
(40) Toupin, M.; Brousse, T.; Be'langer, D. *Chem. Mater.* **2002**, *14*, 3946–3952.
(41) Djurfors, B.; Broughton, J. N.; Brett, M. J.; Ivey, D. G. *Acta Mater.* **2005**, *53*, 957–965.

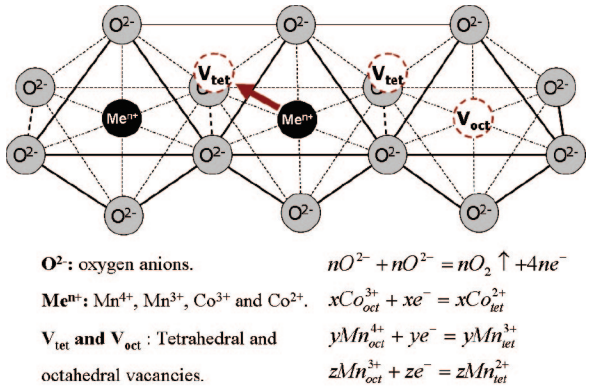

Figure 5. Schematic representation of a possible model for the cation migration and the accompanying chemical reactions during the rock salt−spinel structural transformation. Three octahedral and two nearest neighbour tetrahedral positions in the rock salt-type arrays are highlighted. Because the cation deficiency (percentage of vacancies) in the as-deposited oxides is in the 30–45% range,[22] V_{oct} is assigned to one of the three octahedral positions.

time. Thus far, no experimental evidence has been obtained for these intermediate stages during the phase transformation. In situ TEM analysis is needed to uncover the nature of the rock salt−spinel structural transformation in anodically deposited Mn−Co−O nanocrystals.

Conclusions

The structural transformation for anodically deposited Mn−Co−O nanocrystals, ranging in composition from pure Co oxide to pure Mn oxide, was studied using WDS, XPS, and TEM. WDS and XPS analyses suggest that oxygen evolution and reduction of Co/Mn cations occurred at temperatures as low as 200 °C. As the annealing temperature increases, some of the cations, with higher valences, such as Co^{3+} or Mn^{3+}/Mn^{4+}, were gradually reduced to cations with lower oxidation states, such as Co^{2+} and Mn^{2+}/Mn^{3+}. TEM results indicate that the rock salt−spinel structural transformation occurred in the oxide nanocrystals annealed at a temperature of 500 °C. A cubic $Fd\bar{3}m$ spinel-type structure was obtained for the Co-rich, Mn−Co−O oxide nanocrystals, while a distorted tetragonal-type spinel phase (space group of $I4_1/amd$) formed in their Mn-rich counterparts. The structural transformation involves the migration of Mn/Co cations from the octahedral interstices to the tetrahedral interstices, which is accompanied by the reduction of Mn/Co cations and oxygen evolution. The proposed transformation mechanism is as follows: As the annealing temperature increases, some of the cations in the octahedral interstices have sufficient energy to surpass the energy barrier to migrate to the nearest neighbor tetrahedral vacancies, which will generate additional vacancies in the former octahedral interstices. As the cation vacancy concentration increases, the vacant octahedral sites become unstable and the oxygen anions form paired bonds to generate oxygen gas. Meanwhile, the migrating Mn/Co cations will capture the electrons released from the oxygen evolution reaction to maintain the charge balance in the oxide nanocrystals. Once one-eighth of the tetrahedral interstices in the rock salt-type unit cells is occupied by migrating cations, stable spinel nuclei can form on the oxide particle surfaces. The spinel nuclei will grow and spread, with time, from the surface to the center of the rock salt-type nanocrystals.

Acknowledgment. The authors acknowledge funding contributions from the Natural Sciences and Engineering Research Council (NSERC) of Canada and Versa Power Systems (VPS).

CM703464P